Astron. Astrophys. 145, 157–169 (1985)

ASTRONOMY AND ASTROPHYSICS

Propagation of nonlinear, radiatively damped longitudinal waves along magnetic flux tubes in the solar atmosphere

G. Herbold[1], P. Ulmschneider[1], H. C. Spruit[2], and R. Rosner[3]

[1] Institut für theoretische Astrophysik, Im Neuenheimer Feld 294, D-6900 Heidelberg, Federal Republic of Germany
[2] Max-Planck-Institut für Astrophysik, Karl-Schwarzschild-Strasse 1, D-8046 Garching bei München, Federal Republic of Germany
[3] Harvard Smithsonian Center for Astrophysics, 60 Garden St. Cambridge, MA 02138, USA

Received July 9, accepted November 2, 1984

Summary. For solar magnetic flux tubes we compare three types of waves: Longitudinal MHD tube waves, acoustic tube waves propagating in the same tube geometry but with rigid walls and ordinary acoustic waves in plane geometry. We find that the effect of the distensibility of the tube is small and that longitudinal waves are essentially acoustic tube waves. Due to the tube geometry there is considerable difference between longitudinal waves or acoustic tube waves and ordinary acoustic waves. Longitudinal waves as well as acoustic tube waves show a smaller amplitude growth, larger shock formation heights, smaller mean chromospheric temperature but a steeper dependence of the temperature gradient on wave period.

Key words: magnetic flux tubes – waves – chromosphere

1. Introduction

In this paper we consider the nonlinear, radiatively damped propagation of magnetoacoustic waves in a thin, intense magnetic flux tube embedded in the otherwise field-free solar atmosphere. Magnetoacoustic wave propagation in magnetic flux tubes in the last years has been extensively studied (Defouw, 1976; Roberts and Webb, 1978, 1979; Wilson, 1979, 1980, 1981; Parker, 1979; Wentzel, 1979; Spruit, 1981a, b, 1982; Roberts, 1983; Edwin and Roberts, 1983) particularly in the case of negligible gravity. These treatments usually start from the linearized MHD equations valid for tube geometries. In the case of zero gravity, the wave equation is solved in terms of a wave moving along the vertically-directed tube axis, where the horizontal variation is described in terms of Bessel functions both inside and outside the tube. Suitable matching at the tube boundary allows the construction of the complete wave. There are several wave types possible (see Spruit, 1982; Edwin and Roberts, 1983): a torsional mode, the nonlinear propagation of which has been studied by Hollweg et al. (1982); two transverse modes (also called taut wire or kink mode); and a longitudinal mode (also called axisymmetric or sausage mode), which is the subject of our present study.

Because the longitudinal mode is compressive, it closely resembles acoustic tube waves travelling in rigid funnels and ordinary acoustic waves in its propagation characteristics. For situations of non-negligible gravity, these waves have first been studied by Defouw (1976), who assumed an isothermal atmosphere. This study was subsequently generalized by Roberts and Webb (1978) to non-isothermal atmospheres. Because the pressure perturbation, and thus the wave in the medium outside the flux tube, was neglected to make the problem tractable, both studies are not as general as the previous work on cases of negligible gravity. This approximation was justified by the fact that for cases of negligible gravity and fully built-up external wave fields no mechanical energy is radiated away from the flux tube in horizontal direction if the external sound speed is larger than the tube speed (Spruit, 1982; see also Spruit and Zweibel, 1979). Thus the assumption of a constant pressure boundary which prevents transmission of acoustic energy seems a good approximation for this case. However, in highly nonlinear cases, where the wave amplitudes are not small, and particularly in situations where we have switch-on effects, the interfering wave field outside must be built up by transfer of wave energy to the outside medium; therefore some acoustic damping must occur. This question will be addressed in a separate paper.

Another effect which cannot be described by a linear treatment is shock formation. This is especially interesting for the problem of chromospheric and coronal heating. The heating mechanism for the outer atmosphere of stars is still unknown, but observations of solar and stellar UV and X-radiation fluxes (e.g. Linsky, 1980; Vaiana et al., 1981) have shown that a purely acoustic wave heating theory cannot be correct, and that there is good correlation between heating and the presence of magnetic fields. Because much of the observed UV and X-ray variation from star to star can be explained by different magnetic field coverage and because hydrodynamic shock formation nicely explains the sudded onset of chromospheric radiation loss (Ulmschneider and Stein, 1982) as derived from empirical solar models, it seems appropriate to explore the propagation of compressive modes in the presence of structured magnetic fields.

A systematic comparison of longitudinal tube waves, acoustic tube waves and ordinary acoustic waves in plane geometry has been made by Rae and Roberts (1982) and by Roberts (1981, 1983) in the linear regime. In the present work we compare these three wave types in the nonlinear regime. In particular we are interested in the shock formation properties to explore whether longitudinal tube waves could be a chromospheric heating mechanism.

From purely acoustic work (Ulmschneider et al., 1978; henceforth USKB 78) it is well-known that radiation damping is important in realistic situations. Webb and Roberts (1980) and Roberts (1983) have in fact computed linear tube waves with constant radiative relaxation time τ_R. Although this gives a basic feeling for the properties of radiatively damped longitudinal waves, it is also known that τ_R is a rapidly increasing function of height (Ulmschneider, 1971). In a time-dependent nonlinear

Send offprint requests to: P. Ulmschneider

treatment, such as ours, variable τ_R and even radiative transfer are easily taken into account (USKB 78). In the thin flux tube limit, which we employ here in order to permit a one-dimensional wave calculation, the radiation field of the flux tube can be neglected compared with that of the surrounding atmosphere. As the mean intensity of the radiation field in the flux tube thus is a specified time-independent quantity, the radiation damping function becomes a local quantity and the radiative transfer equation need not to be solved. This results in a much simplified treatment, which we carry out in the following sections.

Our paper is thus structured as follows: in Sect. 2 we describe the basic equations for longitudinal tube waves, and discuss the difference between these waves and acoustic tube waves. Section 3 describes the shock formation. Our fully nonlinear time-dependent calculations are carried out in Sect. 4, in which we describe the numerical scheme used (method of characteristics); the results are described in Sect. 5. Our conclusions are given in Sect. 6. The solutions of the linear theory for the longitudinal waves are summarized in the Appendix.

2. Basic equations

2.1. Longitudinal tube wave equations

The equations which govern the propagation of longitudinal MHD flux tube waves are derived by making the *thin flux tube* approximation (Defouw, 1976; Roberts and Webb, 1979): the variation of the physical variables, such as field strength B, velocity u, pressure p, density ϱ, etc., *across* the tube are assumed to be much smaller than their variations *along* the tube. For simplicity, one assumes a vertical flux tube of axial symmetry and expands the physical variables at the tube axis in a Taylor series in the horizontal direction. Let t be the time, r the horizontal coordinate, z the vertical coordinate and φ the azimuthal angle. Using the series expansion of the system of MHD equations written in cylindrical coordinates and neglecting all φ-dependent terms, as well as all terms of first and higher order in r, the following set of equations is found

$$\frac{\partial}{\partial t}\frac{\varrho}{B}+\frac{\partial}{\partial z}\left(u\frac{\varrho}{B}\right)=0, \tag{1}$$

$$\frac{\partial u}{\partial t}+u\frac{\partial u}{\partial z}+\frac{1}{\varrho}\frac{\partial p}{\partial z}+g=0, \tag{2}$$

$$\frac{B^2}{8\pi}+p=p_e(z), \tag{3}$$

$$\frac{\partial S}{\partial t}+u\frac{\partial S}{\partial z}=\left.\frac{dS}{dt}\right|_{\mathrm{Rad}}. \tag{4}$$

Here g is the gravitational acceleration for which we take the solar value $g=2.736\,10^4\,\mathrm{cm/s^2}$, $p_e(z)$ is the gas pressure of the field free region outside the flux tube and S is the entropy per gram. All units are *cgs*. In Eq. (4) we have neglected Joule, viscous and conductive heating, but retained radiative damping. Equation (1) is a combination of $\nabla\cdot B=0$, the continuity equation and the z-component of the induction equation. Note that taking the external pressure p_e independent of time in Eq. (3) we neglect the inertia of the external medium, as well as acoustic damping and dispersive effects. This assumption was made to allow a one-dimensional time-dependent treatment. Its restrictivenes can only be judged when simultaneous time-dependent calculations in the flux-tube and the external medium become available.

Equations (4) is the energy equation written in the form of an entropy conservation law. Here S is the entropy per gram. For the radiation damping function $\left.\frac{dS}{dt}\right|_{\mathrm{Rad}}$ we use a grey LTE approximation (Ulmschneider et al., 1978; henceforth USKB 78):

$$\left.\frac{dS}{dt}\right|_{\mathrm{Rad}}=\frac{4\pi\kappa}{T}\;(J-\tilde{B}), \tag{5}$$

where

$$\kappa=1.38\cdot 10^{-23}p^{0.74}T^4 \tag{6}$$

is the grey Rosseland opacity per gram fitted to calculations of Kurucz (1979). T is the temperature within the tube which is related to p and ϱ over the ideal gas equation

$$p=\varrho\frac{\mathscr{R}T}{\mu} \tag{7}$$

where $\mathscr{R}=8.3144\,10^7\,\mathrm{erg/K\,mol}$ is the gas constant and $\mu=1.3\,\mathrm{g/mol}$ is the mean molecular weight for a non-ionized gas.

$$J=\frac{\sigma}{\pi}T_e(z)^4 \tag{8}$$

is the adopted mean intensity, T_e is the temperature outside the tube, σ the Stefan-Boltzmann constant and

$$\tilde{B}=\frac{\sigma}{\pi}T^4 \tag{9}$$

is the Planck function. In this treatment of the radiative transfer we assume that the flux tube is optically thin and that the tube is embedded in a radiation field dominated by the external medium. A comparison with the radiation treatments of Webb and Roberts (1980) and of Roberts (1983) who use Newtons law of cooling and a constant radiative relaxation time is given in Appendix B.

2.2. Acoustic tube wave equations

It is instructive to compare the longitudinal tube wave Eqs. (1) to (9) with the similar equations of acoustic waves in a tube with rigid walls of the same geometry. Let A be the cross section of the tube and, a, the geometrical distance along the tube axis at some initial instant t_0. This distance a is called Lagrange coordinate. If the Eulerian coordinate $z(a,t)$ along the tube is assumed to be a function of the Lagrangian coordinate a and time t, the conservation of mass in the tube can be written in the form (index 0 labels quantities at time t_0)

$$\varrho(a,t)A(a,t)dz=\varrho_0(a)A_0(a)da, \tag{10}$$

or

$$\left(\frac{\partial z}{\partial a}\right)_t=\frac{\varrho_0 A_0}{\varrho A}. \tag{11}$$

Differentiating Eq. (11) with respect to t and using

$$u=\left(\frac{\partial z}{\partial t}\right)_a, \tag{12}$$

we have the continuity equation in Lagrangian form

$$\left(\frac{\partial \varrho A}{\partial t}\right)_a+\frac{\varrho^2A^2}{\varrho_0A_0}\left(\frac{\partial u}{\partial a}\right)_t=0. \tag{13}$$

With the usual relations

$$\left(\frac{\partial f}{\partial t}\right)_a = \left(\frac{\partial f}{\partial t}\right)_z + u\left(\frac{\partial f}{\partial z}\right)_t, \tag{14}$$

$$\left(\frac{\partial f}{\partial a}\right)_t = \left(\frac{\partial f}{\partial z}\right)_t \left(\frac{\partial z}{\partial a}\right)_t, \tag{15}$$

used when going over to the Eulerian frame we find from Eq. (13) the Eulerian continuity equation for acoustic tube waves

$$\left(\frac{\partial \varrho A}{\partial t}\right)_z + \left(\frac{\partial \varrho u A}{\partial z}\right)_t = 0. \tag{16}$$

This equation is well-known in the literature of engineering aerodynamics and duct flow (e.g. Rudinger, 1969, p. 12; Lighthill, 1980, p.92). In plane parallel geometry, A is constant and Eq. (16) reduces to the familiar continuity equation (Landau and Lifshitz, 1959, p. 2). The momentum and energy equations for tube waves in Lagrangian form can be written as

$$\varrho_0 A_0 \left(\frac{\partial u}{\partial t}\right)_a + A\left(\frac{\partial p}{\partial a}\right)_t + \varrho_0 A_0 g = 0, \tag{17}$$

and

$$\left(\frac{\partial S}{\partial t}\right)_a = \left.\frac{dS}{dt}\right|_{\text{Rad}}. \tag{18}$$

Here $\varrho_0 A_0$ is the mass element (g/cm); the pressure force acts on the actual cross section A. With Eqs. (14) and (15) it is easily seen that the Eulerian forms of (17) and (18) are identical to Eqs. (2) and (4).

2.3. *Differences between longitudinal and acoustic tube waves*

As the magnetic flux in a flux tube is concerved we have

$$BA = \Phi = \text{const}. \tag{19}$$

With this relation it is seen that the continuity equations (1) and (16) are identical; and similarly for the momentum and energy equations. However, because B can be eliminated from Eq. (3) in favour of A, it is clear that longitudinal MHD tube waves are acoustic tube waves with a specific "breathing law", which specifies the variation of the tube cross section with gas pressure. The distensibility of the tube adds an additional restoring force to the volume compressibility and thus alters the propagation speed of the wave (Lighthill, 1980, p. 93). Note that this distensibility is not a wall effect like in human blood vessels but is a volume effect. For the propagation speed in the longitudinal tube wave one has from Eqs. (3), (19)

$$c_T^2 = \frac{1}{\varrho(\mathscr{K}+\mathscr{D})} = \frac{1}{\varrho\left(-\frac{1}{V}\frac{\partial V}{\partial p}\Big|_S + \frac{1}{A}\frac{\partial A}{\partial p}\Big|_S\right)} = \frac{c_S^2 c_A^2}{c_S^2 + c_A^2}. \tag{20}$$

Here $V = \varrho^{-1}$ is the specific volume, $\mathscr{K}$ the adiabatic compressibility, $\mathscr{D}$ the adiabatic distensibility, c_S the sound speed and c_A the Alfvén speed. It is seen that while in a rigid acoustic tube wave the propagation speed is the sound speed, the propagation speed c_T of the longitudinal tube wave is always less than both c_A and c_S. In addition to the modification of the propagation speed, the ordinary acoustic wave, the acoustic tube wave and the longitudinal tube wave differ in the acoustic cut-off frequency ω_c. As this has already been found by Defouw (1976) and e.g. by Rae and Roberts (1982) we do not repeat a discussion here.

3. Shock waves

We now consider the formation of shocks as compressive tube waves propagate down a density gradient.

3.1. *Hugoniot relations for longitudinal tube waves*

Purely hydrodynamic shocks occur over distances of the order of the molecular mean free path

$$l = \frac{1}{nq}, \tag{21}$$

which in the low chromosphere is about 10 cm. Here n is the number density of the gas and q is the hydrogen collision cross section, which in the low chromosphere can be written

$$q = \pi(2a_0)^2, \tag{22}$$

where a_0 is the Bohr radius. As the typical length scale for acoustic waves is of the order of the scale height, which is in the range of 10^7 cm, it is a good approximation to represent a hydrodynamic shock by a discintinuity. For longitudinal tube waves we now assume that the region where the strong bending of magnetic field lines near the hydrodynamic shock occurs is very small compared to the typical length scale of the acoustic waves, but is also considerably larger than l. In addition, we disregard for the moment the occurrence of modecoupling in the near shock region; this will be discussed in a subsequent paper. The Hugoniot relations for longitudinal tube waves may then be derived as follows. Consider the shock discontinuity in a frame comoving with the shock (see Fig. 1). At the front the gas enters the shock with velocity v_1, density ϱ_1 and pressure p_1. The tube cross section is A_1. At the back the gas leaves with velocity v_2, density ϱ_2 and pressure p_2. The tube cross section is now A_2. Let us assume that the longitudinal tube wave equations are written in the frame comoving with the shock. We integrate the continuity Eq. (16) over the discontinuity from height z_2 to z_1. Take the time derivative of the first term out of the integral; because ϱA is bounded, we see that this integral vanishes for $z_1 - z_2 \to 0$. From the second term of Eq. (16) we get the first Hugoniot relation

$$\varrho_1 v_1 A_1 = \varrho_2 v_2 A_2, \tag{23}$$

Multiplying Eq. (16) with v and Eq. (2) with ϱA and adding, we have

$$\frac{\partial}{\partial t}(\varrho v A) + \frac{\partial}{\partial z}(\varrho v^2 A) + A\frac{\partial p}{\partial z} + \varrho A g = 0. \tag{24}$$

From Eq. (3) and (19) we have

$$A = \phi[8\pi(p_e - p)]^{-1/2}, \tag{25}$$

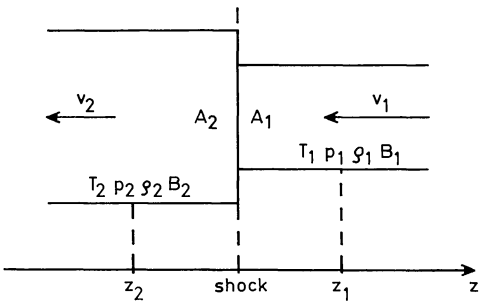

Fig. 1. Physical quantities in front of (labeled 1) and behind (labeled 2) the shock in a frame comoving with the shock

and

$$A\frac{\partial p}{\partial z}=-2\frac{\partial}{\partial z}[A(p_e-p)]+A\frac{dp_e}{dz}. \tag{26}$$

Thus the momentum conservation equation can be written

$$\frac{\partial}{\partial t}(\varrho vA)+\frac{\partial}{\partial z}[(\varrho v^2-2p_e+2p)A]+A\frac{dp_e}{dz}+\varrho gA=0. \tag{27}$$

Integrating from z_2 to z_1 we find again that the integrands of the first, third, and fourth term are bounded and vanish for $(z_1-z_2)\to 0$. We thus have the second Hugoniot relation,

$$A_1(\varrho_1 v_1^2-2p_e+2p_1)=A_2(\varrho_2 v_2^2-2p_e+2p_2). \tag{28}$$

For the derivation of the energy conservation equation we consider

$$\frac{\partial}{\partial t}\left[\left(\frac{1}{2}\varrho v^2+\varrho E+\varrho\phi\right)A\right]$$
$$=\frac{1}{2}v^2\frac{\partial(\varrho A)}{\partial t}+\varrho vA\frac{\partial v}{\partial t}+\frac{\partial(\varrho EA)}{\partial t}+\frac{\partial(\varrho\phi A)}{\partial t}, \tag{29}$$

where E is the specific internal energy and $\phi=\phi_0+gz$ is the gravitational potential, with ϕ_0 a constant. Following Landau and Lifshitz (1966, p. 247) we use Eqs. (2) and (16) as well as the thermodynamic relations to modify the right-hand side of Eq. (29). Assuming that ϕ is time-independent, we find after some algebra that

$$\frac{\partial}{\partial t}\left[\left(\frac{1}{2}\varrho v^2+\varrho E+\varrho\phi\right)A\right]$$
$$+\frac{\partial}{\partial z}\left[\varrho vA\left(\frac{1}{2}v^2+W+\phi\right)\right]+p\frac{\partial A}{\partial t}=0, \tag{30}$$

where W is the specific enthalpy. With Eq. (25) and $\frac{\partial p_e}{\partial t}=0$ we have

$$p\frac{\partial A}{\partial t}=\frac{\partial(2p_eA)}{\partial t}-\frac{\partial(pA)}{\partial t}, \tag{31}$$

and with Eq. (3) obtain the energy conservation equation

$$\frac{\partial}{\partial t}\left[\left(\frac{1}{2}\varrho v^2+\varrho E+\frac{B^2}{8\pi}+p_e+\varrho\phi\right)A\right]$$
$$+\frac{\partial}{\partial z}\left[\varrho vA\left(\frac{1}{2}v^2+W+\phi\right)\right]=0. \tag{32}$$

The first term on the left hand side contains the kinetic, internal and magnetic energy densities, as well as the potential energy densities due to the tube wall distension and to gravity. The second term contains the energy flux, which is unchanged compared to the plane parallel and the spherically symmetric cases. As the first term again vanishes upon integration from z_2 to z_1 and going over to the limit $(z_1-z_2)\to 0$, we have the ordinary third Hugoniot relation

$$\tfrac{1}{2}v_1^2+W_1=\tfrac{1}{2}v_2^2+W_2. \tag{33}$$

The three Hugoniot relations (23), (28), and (33) can be used to connect the continuous regions, where the longitudinal tube wave equations apply, across the shock. To transform the Hugoniot relations into the Eulerian frame, we use

$$v_1=u_1-U_{SH}, \tag{34}$$

$$v_2=u_2-U_{SH}, \tag{35}$$

where U_{SH} is the shock velocity in the Eulerian frame. The shock velocity in the Lagrangian frame is, e.g.,

$$\left(\frac{\partial a}{\partial t}\right)_{SH}=(U_{SH}-u_1)\left(\frac{\partial a}{\partial z}\right)_{t,1}, \tag{36}$$

where 1 labels the region in front of the shock.

3.2. *Hugoniot relations for acoustic tube waves*

As the tube cross section does not change across the shock for acoustic tube waves in rigid tubes, the Hugoniot relations (23, 28, and 33) for these waves reduce to the ordinary Hugoniot relations (Landau and Lifshitz, 1959, p. 319). These relations can be obtained by going to the limit of very small distensibility, e.g., $\xi\ll 1$ where

$$\xi\equiv\frac{p}{p_e}. \tag{37}$$

From Eq. (25) we have to first order

$$A\simeq\text{const}\,p_e^{-1/2}(1+\tfrac{1}{2}\xi) \tag{38}$$

which, when inserted in Eqs. (23) and (28), leads to the ordinary Hugoniot relations in the limit $\xi\to 0$.

3.3. *Solution of the Hugoniot relations*

In the time-dependent work described in the next section it is necessary to solve the Hugoniot relations a considerable number of times. It thus is important to develop an efficient method of solution. For this solution the physical variables u_1, c_{S_1}, S_1, p_1, ϱ_1, W_1, A_1, p_e in front of the shock are known in addition to the post shock velocity u_2. Together with the thermodynamic relations

$$W=\frac{c_S^2}{\gamma-1}, \tag{39}$$

$$c_S^2=\gamma\frac{p}{\varrho}, \tag{40}$$

and

$$\frac{\varrho_2}{\varrho_1}=\left(\frac{c_{S_2}}{c_{S_1}}\right)^{\frac{2}{\gamma-1}}e^{-\frac{\mu(S_2-S_1)}{\mathscr{R}}}, \tag{41}$$

valid for a non-ionizing ideal gas, Eqs. (23), (25), (28), and (33)–(35) are sufficient to determine the 9 unknows c_{S_2}, S_2, p_2, ϱ_2, W_2, A_2, v_1, v_2, U_{SH}. Eliminating all unknowns except A_2, one is able to derive a third order equation for A_2,

$$E_0+E_1A_2+E_2A_2^2+E_3A_2^3=0, \tag{42}$$

where, by defining $\Delta u\equiv u_2-u_1$, one has

$$E_0=\frac{\gamma-2}{\gamma-1}\Delta u^2\varrho_1^2A_1^4, \tag{43}$$

$$E_1=\Delta u^2\varrho_1^2A_1^3\left[\frac{4-3\gamma}{\gamma-1}-\frac{4\pi}{\Phi^2}\Delta u^2\varrho_1\frac{A_1^2}{\gamma-1}-\frac{8\pi}{\Phi^2}W_1\varrho_1A_1^2\right], \tag{44}$$

$$E_2=2\Delta u^2\varrho_1^2A_1^2\left[1-\frac{2\pi}{\Phi^2}\Delta u^2\varrho_1A_1^2\right.$$
$$\left.+\frac{\gamma}{\gamma-1}\frac{4\pi}{\Phi^2}p_eA_1^2+\frac{4\pi}{\Phi^2}W_1\varrho_1A_1^2\right], \tag{45}$$

$$E_3=\frac{\gamma}{\gamma-1}\frac{8\pi}{\Phi^2}\Delta u^2p_e\varrho_1^2A_1^3\left[\frac{4\pi}{\Phi^2}\Delta u^2\varrho_1A_1^2-1\right]. \tag{46}$$

Of the three solutions of Eqs. (42), the first is negative and the second is smaller than A_1. They are thus both unphysical, for the latter because of the pressure increase associated with the entropy jump. The correct solution is the largest root A_2 which is found by Newton's method. In cases where the shock is still weak, the two positive solutions are very close together but can be separated by determining the point of zero slope between the two solutions from Eq. (42). The remaining unknowns can be found by using

$$\varrho_2 = \frac{\varrho_1 A_1}{A_2}\left[\frac{A_1 - A_2}{\frac{4\pi}{\Phi^2}\Delta u^2 \varrho_1 A_1^2 A_2 + A_1 - A_2}\right], \tag{47}$$

$$v_1 = -\frac{\varrho_2 A_2 \Delta u}{\varrho_2 A_2 - \varrho_1 A_1}, \tag{48}$$

$$v_2 = -\frac{\varrho_1 A_1 \Delta u}{\varrho_2 A_2 - \varrho_1 A_1}, \tag{49}$$

and Eqs. (25), (34), and (39)–(41).

4. Time-dependent non-linear calculations: method

The discussion of the solution of the linear longitudinal MHD tube wave equations has already been given by Defouw (1976), by Roberts and Webb (1978) and others. The purpose of our present work is to make a detailed comparison with acoustic tube waves as well as with ordinary acoustic waves both for linear and non-linear cases and to derive the phase relations. For this reason the linear solutions are discussed in the Appendix.

4.1. *Initial atmosphere, flux tube model*

Time-dependent calculations can start from any initial state consistent with the dynamical equations. As we want to study primarily the properties of longitudinal tube waves, and not the global behaviour of the solar atmosphere, it is therefore advantageous to start from an initial atmosphere which, in absence of waves, does not show time dependence. This is a radiative equilibrium atmosphere.

Following our previous work on acoustic waves (e.g., USKB 78) we adopt a grey radiative equilibrium atmosphere outside the flux tube. As the regions between the flux tubes may be quite cool (Ayres, 1981), such a model which neglects the chromospheric temperature rise seems quite appropriate for the external medium. With external pressure p_e and temperature T_e thus given as function of height, the time independent static versions of Eqs. (2), (3), (7), and (19) with $T_0 = T_e$ can then be solved for B_0, p_0 and A_0 as functions of height if B_{00} and A_{00} are specified at the bottom of the flux tube. For the magnetic field strength B_{00} and the tube cross section A_{00} typical values are used which were determined empirically (Zwaan, 1978; Stenflo, 1978). As costumary the zero height level ($z = 0$) at the bottom of the tube is taken where the external atmosphere has optical depth unity at 500 nm. The non-uniform grid spacing Δz is chosen such that the wave is well-resolved, and such that there are enough height points per scale height (see Ulmschneider et al., 1977). The resulting initial flux tube model (dashed) is exhibited in Fig. 2, it is called model *A*.

The crowding of the flux tubes at the (super-) granulation boundaries does not permit an exponential horizontal spreading of individual tubes to go on indefinitely. To take into account this effect we have constructed model *B* which above a height $z_0 = 500$ km spreads only linearly with height. As the grey radiative equilibrium atmosphere external to the flux tube has an isothermal boundary temperature with scale height H we assume using

$$A_0 = A_{00} e^{-z/2H} \tag{50}$$

for $z > z_0$ that the tube radius increases linearly as

$$r = r_0 + \frac{r_0}{4H}(z - z_0) \tag{51}$$

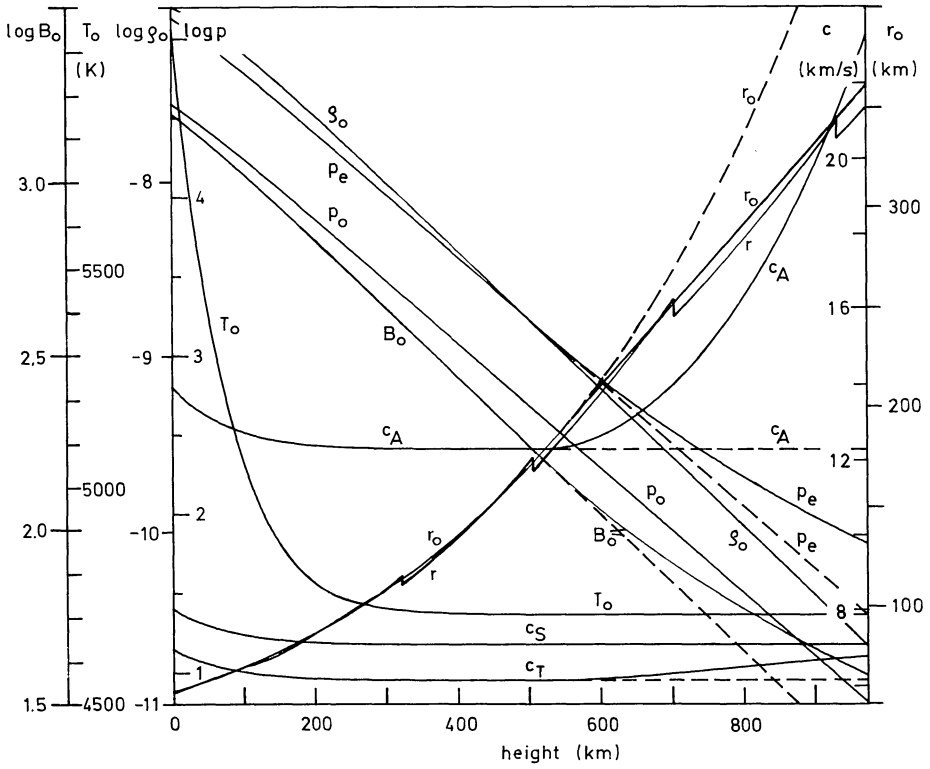

Fig. 2. Initial flux tube model *A* (dashed) and model *B* (solid). The magnetic field strength B_0 is given in (*G*), the gas pressure p in (dyn/cm^2) and the density ϱ_0 in (g/cm^3). The other quantities are defined in the text. r shows the instantaneous tube radius of the wave of Fig. 4

from which the magnetic field strength B_0 can be calculated using Eq. (19). For $z>z_0$ the horizontal pressure balance Eq. (3) in the model construction is thus replaced by

$$p+\frac{\Phi^2}{8\pi^3\left(r_0+\frac{r_0}{4H}(z-z_0)\right)^4}=p_e(z) \tag{52}$$

from which a modified external pressure $p_e(z)$ is computed which supposedly takes into account external magnetic stresses. Model B (drawn) is shown in Fig. 2. From this figure it is seen that the Alfvén speed c_A is always a factor of between 2 and 3 greater than the sound velocity c_S; for this reason the tube speed c_T closely follows c_S. The tube spreads from a radius of $r=57$ km at height $z=0$ to $r=167$ km at $z=500$ km, and $r=849\,(663)$ km at $z=900$ km; the value in brackets is for model B. In model A, the gas pressure p_0 inside the tube is reduced by a factor of 3.5 compared to p_{e0}, while toward the top of model B it decreases more rapidly.

4.2. *Method of characteristics*

In order to numerically solve the longitudinal tube wave equations we follow our work on acoustic waves (Ulmschneider et al., 1977), and select the method of characteristics. This method has been shown (Hammer and Ulmschneider, 1978) to be much more efficient than finite difference methods for problems of the sort we deal with here; in addition, it allows shock finding and a detailed shock treatment. In this method, the system of three partial differential Eqs. (1), (2), (4) in Eulerian form, or (13), (17), (18) in Lagrangian form are written as a system of 6 ordinary differential equations, of which 3 equations describe the three characteristics (C^+, C^-, C^0). After some algebra similar to that for acoustic waves (Ulmschneider et al., 1977), we find for these ordinary differential equations in Lagrangian form

$$du\pm\frac{2}{\gamma-1}\frac{c_S}{c_T}dc_S\mp\frac{\mu c_S^2}{\gamma\mathscr{R}c_T}dS\mp\left(\frac{\mu c_T}{\gamma\mathscr{R}}(\gamma-1)\frac{dS}{dt}\bigg|_{\text{Rad}}+\frac{uc_T}{\varrho c_A^2}\frac{dp_e}{dz}\mp g\right)dt=0 \tag{53}$$

along the characteristics, which are given by

$$\frac{da}{dt}=\pm c_T\frac{\varrho A}{\varrho_0 A_0}. \tag{54}$$

Here the upper sign is for the C^+, and the lower for the C^- characteristic. The energy equation gives

$$dS=\frac{dS}{dt}\bigg|_{\text{Rad}}dt \tag{55}$$

along the C^0 characteristic, $a=$const.

For the case of acoustic tube waves with rigid walls we find instead

$$du\pm\frac{2}{\gamma-1}dc_S\mp\frac{\mu c_S}{\gamma\mathscr{R}}dS\mp\left(\frac{\mu c_S}{\gamma\mathscr{R}}(\gamma-1)\frac{dS}{dt}\bigg|_{\text{Rad}}-\frac{uc_S}{A_0}\frac{dA_0}{dz}\mp g\right)dt=0 \tag{56}$$

along

$$\frac{da}{dt}=\pm c_S\frac{\varrho A}{\varrho_0 A_0}. \tag{57}$$

For constant A these equations go over to the ordinary acoustic waves in gravitationally-stratified atmospheres. The details of the numerical solution procedure and boundary conditions are similar to the purely acoustic case, and are described by Ulmschneider et al. (1977).

4.3. *Wave flux*

As the energy flux in Eq. (32) is identical to that in ordinary acoustic waves, the wave flux can be similarly derived (Landau and Lifshitz, 1959, p. 251) as

$$F_M=\overline{p'u} \tag{58}$$

where the bar denotes a time mean and the prime the difference between the actual and the time averaged value. As for adiabatic waves, the total wave energy flux A_0F_M is conserved; we thus see from Eqs. (50), (A.2), and (A.4) that the exponential steepening behaviour of the solution is a consequence of energy conservation. For $\omega\gg\omega_c$ or $k\gg 0$ one finds from the phase relations (A.7), (A.8), and (A.10) that the wave amplitudes are connected by

$$\frac{p'}{\varrho'}=\frac{p_0}{\varrho_0}\frac{\tilde{p}}{\tilde{\varrho}}\simeq c_S^2,\qquad \frac{\varrho'}{u}=\frac{\varrho_0\tilde{\varrho}}{\tilde{u}}\simeq\frac{\varrho_0 c_T}{c_S^2}. \tag{59}$$

Thus in the limit $\omega\gg\omega_c$ the wave flux is given by

$$F_M=\varrho_0 c_T\overline{u^2}. \tag{60}$$

In the present work we used Eq. (60) and adopted a piston velocity

$$u=-u_0\sin\left(\frac{2\pi}{P}t\right), \tag{61}$$

where P is the wave period and the initial wave amplitude is

$$u_0=\left(\frac{2F_M}{\varrho_{00}c_{T0}}\right)^{1/2}. \tag{62}$$

Here ϱ_{00} and c_{T0} are values at the bottom of the flux tube.

5. Time-dependent non-linear calculations: results

In this section, we discuss the nature of the solutions obtained from our numerical simulations of compressible tube waves.

5.1. *General properties of radiatively damped longitudinal tube waves*

Figures 3–6 show computed wave profiles obtained for cases of a fixed mechanical flux $F_M=1.5\,10^8$ erg/cm^2 s and various wave periods $P=20, 30, 45, 60$ s. For ready comparison these figures are plotted on the same scale. The flux tube is that of model B. A comparison with the purely acoustic wave computations of USKB 78 shows at first a strikingly similar overall behaviour, but there are interesting differences in the details. First, the velocity, u, pressure, p, and temperature, T, amplitudes increase much less steeply with height in the tube calculations, a result which is due to the tube spreading [cf. Eqs. (A.2)–(A.4)]. Second, the amplitude of the radiation damping function $D=\frac{dS}{dt}\Big|_{\text{Rad}}$ decreases much more rapidly with height in the tube calculations when compared to the results of USKB 78; this difference is due to the much lower gas pressure in the flux tube and to the fact that in the present results,

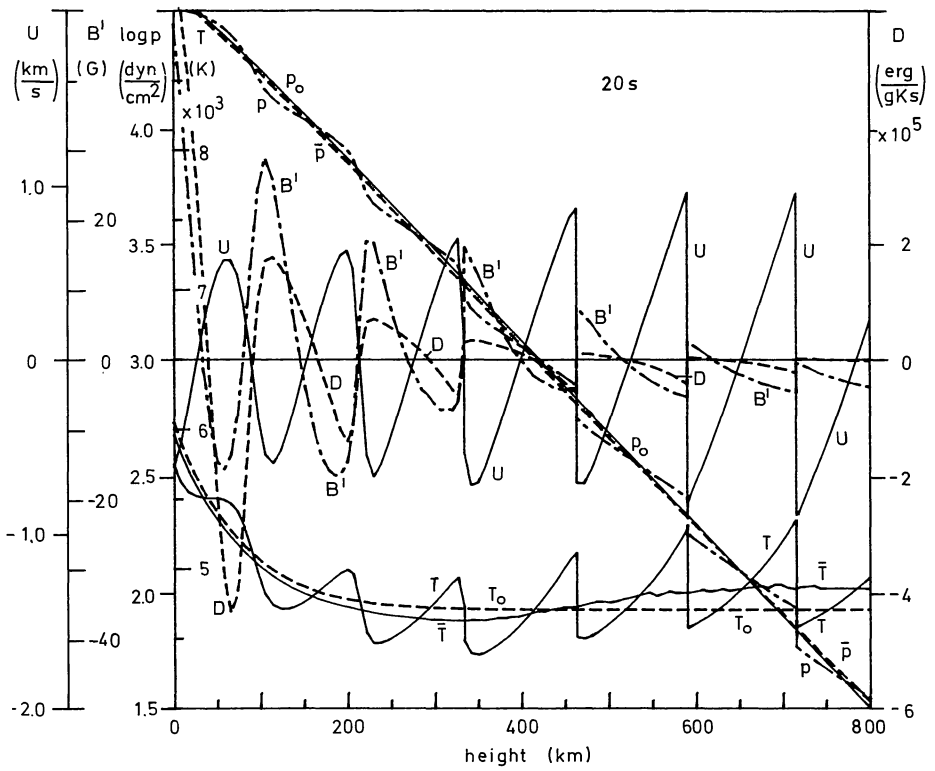

Fig. 3. Longitudinal tube wave of period $P=20$ s and initial flux $F_M=1.5\,10^8$ erg/cm^2 s at time $t=1084$ s. The physical quantities (defined in the text) are shown as function of the Eulerian height z

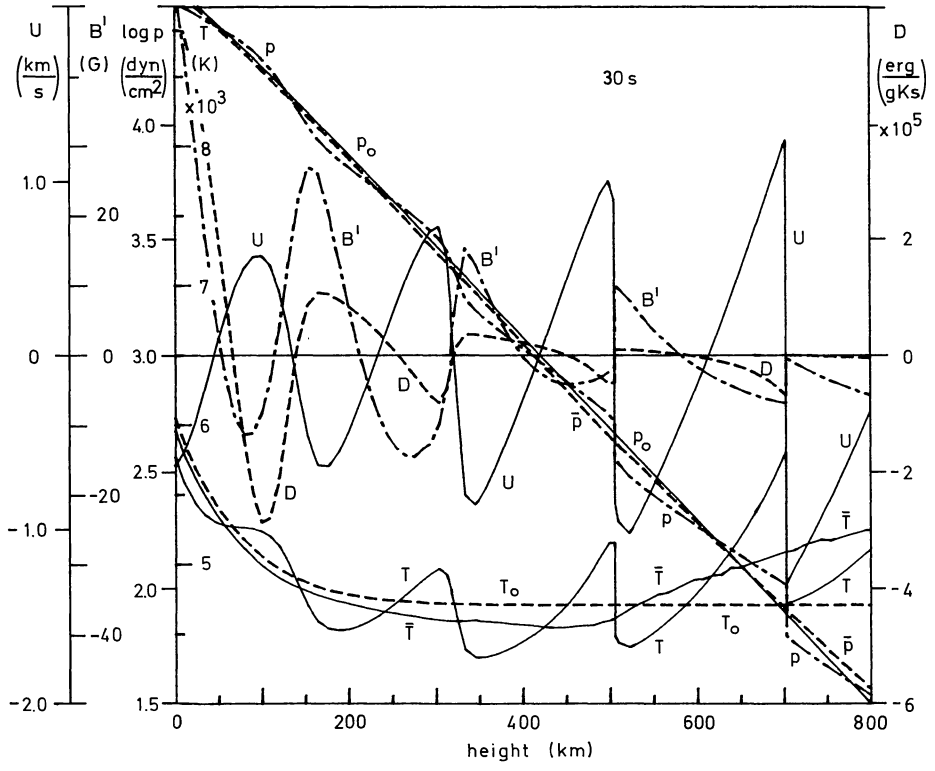

Fig. 4. Same as Fig. 3, however for $P=30$ s at time $t=1567$ s

the weakly increasing temperature oscillations do not strongly oppose the rapid decay of the opacity with height. This effect is especially apparent at greater heights, where in spite of the T^8 temperature dependence [cf. Eqs. (6) and (9)] the radiative emission behind the shocks is greatly decreased compared to the USKB 78 results.

The phase shifts between the physical variables are similar to the pure acoustic case, and are dominated by the short period ($\omega \gg \omega_c$) behaviour. The oscillations of the pressure, p, velocity, u, and temperature, T, are in phase [cf. Eqs. (A.8)–(A.10)], while the damping function D is 180° out of phase with T, as is expected from Eqs. (5), (9) for an optically thin situation. The time-averaged

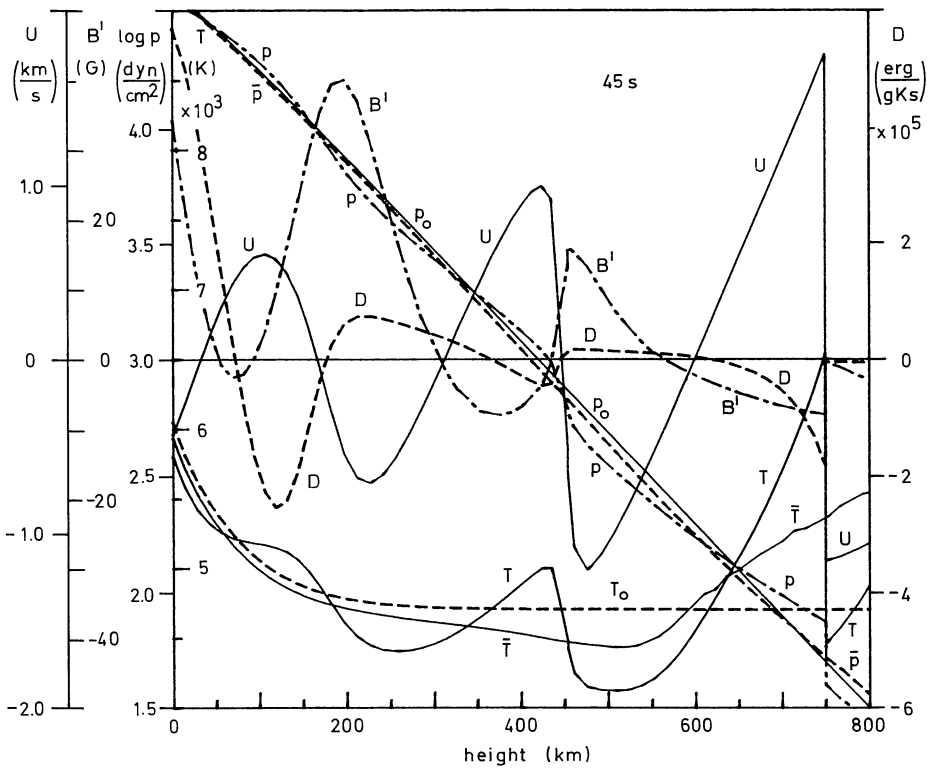

Fig. 5. Same as Fig. 3, however for $P=45$ s at time $t=1895$ s

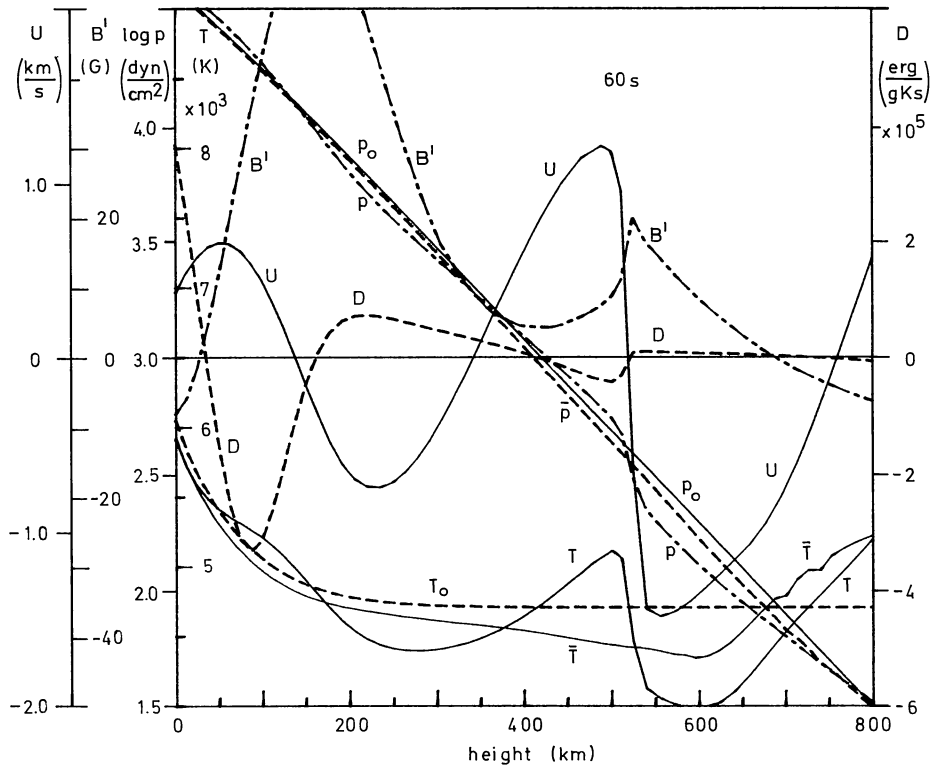

Fig. 6. Same as Fig. 3, however for $P=60$ s at time $t=1194$ s

temperature, $\bar{T}$, behaves quite similarly to the cases of USKB 78. At heights lower than the temperature minimum, the mean temperature is depressed below the initial radiative equilibrium temperature, T_0, due to the non-linearity of the Planck-function, as explained by USKB 78. Above the temperature minimum, shock dissipation raises the mean temperature significantly. However, due to the weakly increasing wave amplitude and consequently decreased dissipation rate, the chromospheric temperature rise is much smaller for longitudinal tube waves. This again is due to the spreading of the flux tube, which keeps the shock strength small.

The temperature minima in Figs. 3–6 occur at progressively greater heights as the wave period is increased. This is expected

from the increase of the shock formation height, z_{SH}, with wave period (cf. Sect. 5.3, below). For short period waves the increase of $\bar{T}$ due to shock dissipation occurs at low height where small temperature excesses generate significant radiation losses. Thus the 20 s wave spends most of its mechanical energy at low height. At greater height the tube spreading and the low mechanical flux lead to weak shocks and thus to only an insignificant chromospheric temperature rise. With larger wave period and therefore higher z_{SH}, the amount of mechanical energy available at greater heights is increased, leading to stronger shocks and consequently to steeper chromospheric temperature gradients (cf. Figs. 3–6).

5.2. *Wave pressure, magnetic field perturbation and tube cross section*

Another rather interesting quantity in the present calculation is the time-averaged pressure $\bar{p}$. Consider the case of hydrostatic equilibrium where the first term in Eq. (17) can be neglected and where after integrating over the appropriate atmospheric slab one has

$$\bar{p} = -\int_a^\infty \frac{\overline{\varrho_0 A_0 g}}{A} da = -\int_a^\infty \varrho_0 g da = p_0 . \tag{63}$$

This shows that in the case of hydrostatic equilibrium, $\bar{p}$ at a Lagrangian height always stays equal to the pressure of the initial atmosphere at that height. Here $\bar{p}$ is essentially gravity times the mass column density of the atmospheric slab above the considered height. In our present calculation, however, where hydrostatic equilibrium is replaced by the dynamical equilibrium, wave pressure augments gas pressure, and consequently $\bar{p} < p_0$ in the dynamically steady state. Moreover, the mass zones are displaced in the Eulerian frame as a consequence of heating and cooling processes. Thus, at low heights in the Eulerian frame the effects of the temperature depression and wave pressure combine to decrease $\bar{p}$ (cf. Figs. 3–6). At greater heights, shock heating expands the atmosphere and thus $\bar{p}$ becomes larger than the initial pressure at that height. This has also been found for purely acoustic waves (USKB 78).

The height dependence of $\bar{p}$ helps us to understand the behavior of the magnetic field oscillation B'. In Figs. 3–6 $B' = B(z,t) - B_0(a)$ is shown in the Eulerian frame; it is seen that B' is nonsymmetric. This effect is explained by the behaviour of the time averaged pressure $\bar{p}$. At low heights where $\bar{p} < p_0$ the magnetic field after Eq. (3) oscillates around a value $\bar{B} > B_0$ while at greater heights where $\bar{p} > p_0$ one has $\bar{B} < B_0$. As p and u are correlated, the B' oscillation is 180° out of phase with u.

Another interesting quantity is the tube cross section A. After Eq. (19) the oscillations in cross section, A', and B' are 180° out of phase with one another; but A is in phase with p [cf. Eq. (25)]. The actual tube cross section as function of height for the same wave and instant of Fig. 4 is shown in Fig. 2. As expected it is seen that the tube cross section is always larger in the high pressure area behind the shock. At greater heights, as consequence of wave heating which leads to $\bar{p} > p_0$, the tube cross section is expanded beyond the original configuration (cf. Fig. 2).

5.3. *Shock formation heights*

Figure 7 shows shock formation heights of a large number of wave calculations for different wave energy flux F_M and period P in flux tube model B, obtained in cases with and without radiation damping. In addition to the results for longitudinal tube waves (solid), shock heights for acoustic tube waves (dashed) and for ordinary acoustic waves (dash-dot) are shown. All waves are calculated for the same initial atmospheric density and temperature distribution; that is, the density ϱ_{00} at the bottom of the atmosphere was the same in all calculations. As a general rule, it is seen that the shock heights increase with period for all wave types. This is due to the fact that the non-linear effects, which depend on the wave amplitude and distort the wave profile, take much longer to produce shocks when the wavelength is large.

Let us now compare the results for the three types of waves. In the adiabatic case (Fig. 7), the shock heights for longitudinal tube waves and the acoustic tube waves are almost identical. The acoustic tube wave has, however, systematically greater shock heights because this wave has a slightly larger propagation speed, and thus a larger wave length. In addition, the acoustic tube wave has a smaller initial velocity amplitude for the same F_M because $c_T < c_S$ [cf. Eq. (62)]. Both effects lead to greater shock heights.

A comparison between the acoustic tube wave and the ordinary acoustic wave shows the influence of the tube geometry. The spreading tube decreases the mechanical flux and with it the wave amplitude, which leads to greater shock heights. Thus, the tube waves have systematically greater shock heights. The spreading of the flux tube is small at low heights, and thus the shock heights for high initial wave fluxes are rather similar for the three types of waves. At greater heights, however, the geometry effect is very pronounced, leading to a great disparity between the shock heights of tube waves and of ordinary waves.

Radiation damping occurs only at low heights. This leads to a considerable decrease of the wave amplitude, and thus as Fig. 7 shows to an increase of the shock heights. As the spreading of the flux tube affects the wave amplitude further, there is an especially large disparity between adiabatic and radiatively damped waves of low initial wave flux. The pronounced damping of short period waves found in earlier work on ordinary acoustic waves (Ulmschneider et al., 1977, and USKB 78) is not encountered in our present calculations. In the previous work, the short period waves were primarily affected because of the validity of the diffusion approximation,

$$J - \tilde{B} \approx \tfrac{1}{3} \frac{d^2 \tilde{B}}{d\tau^2} , \tag{64}$$

in Eq. (5). For short period waves the term on the right-hand side of Eq. (64) is quite large. As the optical depth, τ, in the flux tube is about a factor of ten smaller than that of the external medium, the diffusion approximation is no longer valid, and thus radiation damping is less strongly period-dependent. In addition, our tube waves are much less affected by radiation damping than the acoustic waves of the earlier calculation because of the low tube density.

5.4. *Tubes of different field strength and spreading*

The results discussed above were for flux tube model B where for heights greater than $z_0 = 500$ km only linear spreading was permitted (cf. Fig. 2). In the interior of supergranulation cells, however, where flux tubes are less crowded, individual tubes usually have more room for spreading. In model A we have assumed that exponential spreading continues to $z_0 > 1000$ km (cf. Fig. 2). Here obviously the thin flux tube approximation $B_r \ll B_z$ becomes quite bad. Figure 8 shows waves with $P = 30$ s and $F_M = 1.5\,10^8$ erg/cm^2 s computed in models A and B, both displayed at the same time $t = 1567$ s. As the shock formation height is

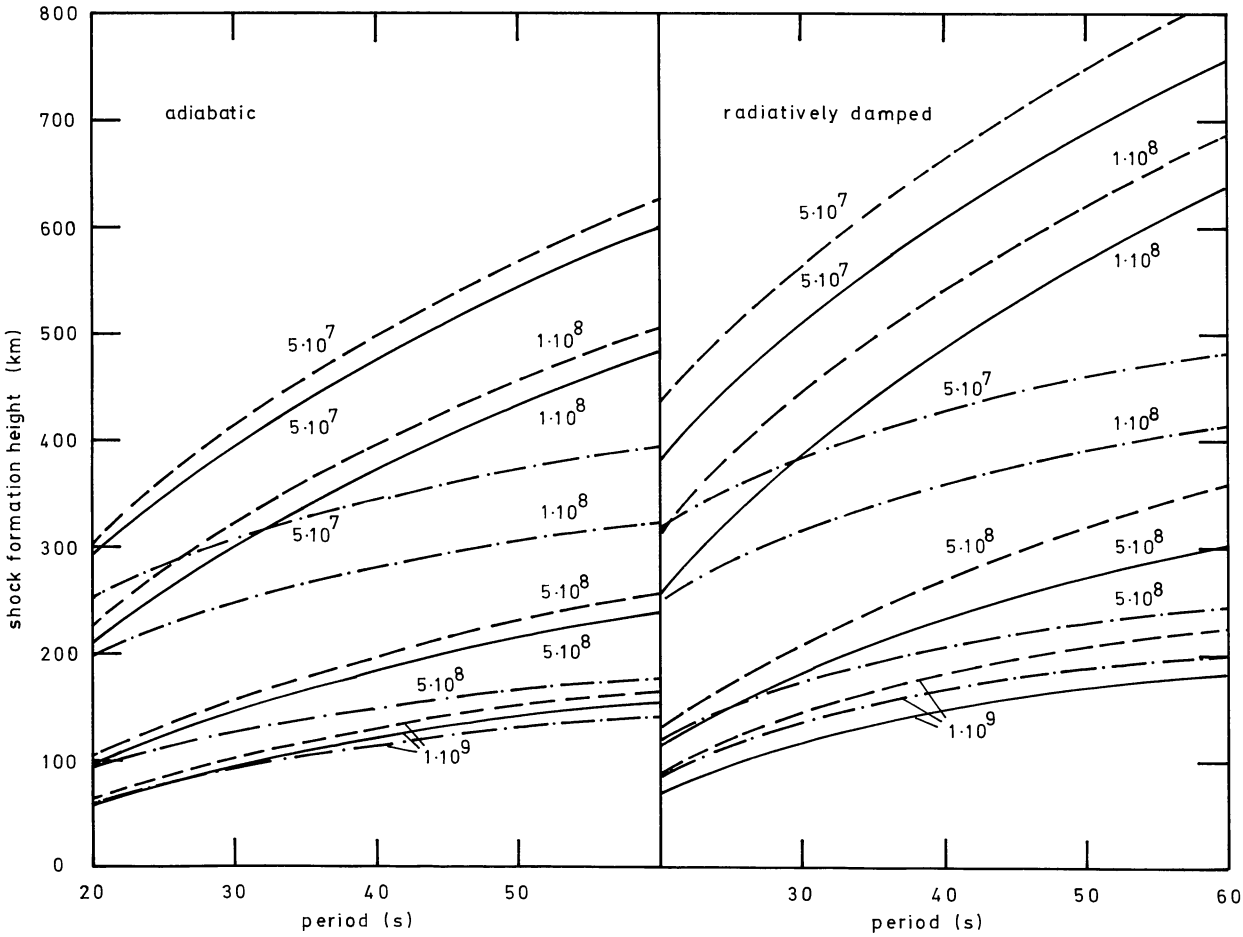

Fig. 7. Shock formation heights for different types of waves as function of wave period P and initial flux F_M (indicated in erg cm^{-2} s^{-1}). Longitudinal tube waves (solid), acoustic tube waves (dashed) and ordinary acoustic waves (–·–·). Left panel: adiabatic waves. Right panel: radiatively damped waves

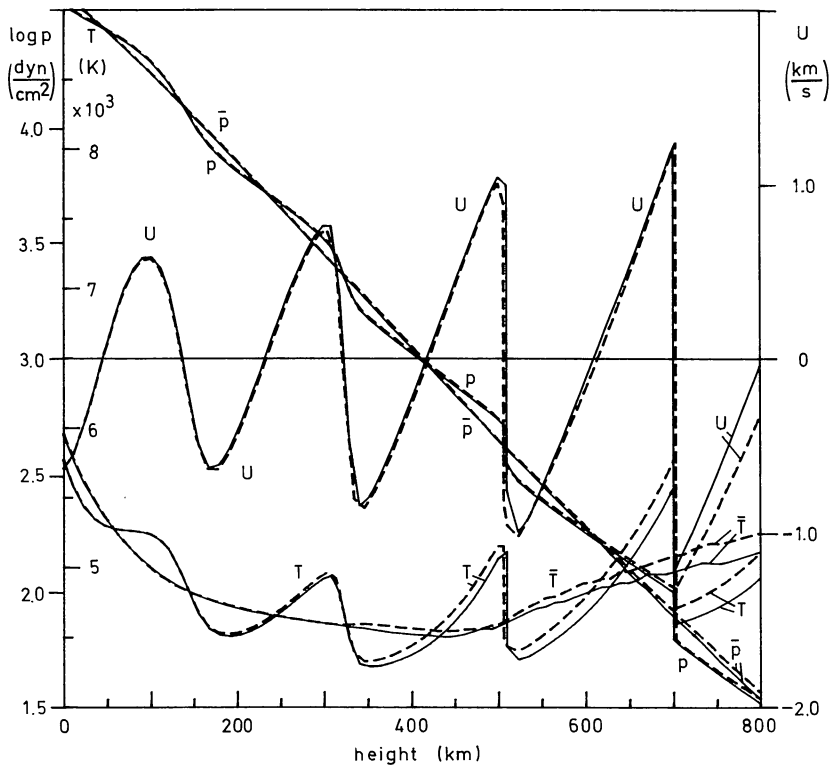

Fig. 8. Wave calculations in flux tube models A (solid) and B (dashed). For comparison both waves with period $P=30$ s and flux $F_M=1.5\,10^8$ erg/cm^2 s are shown at the same time $t=1567$ s (cf. Fig. 4)

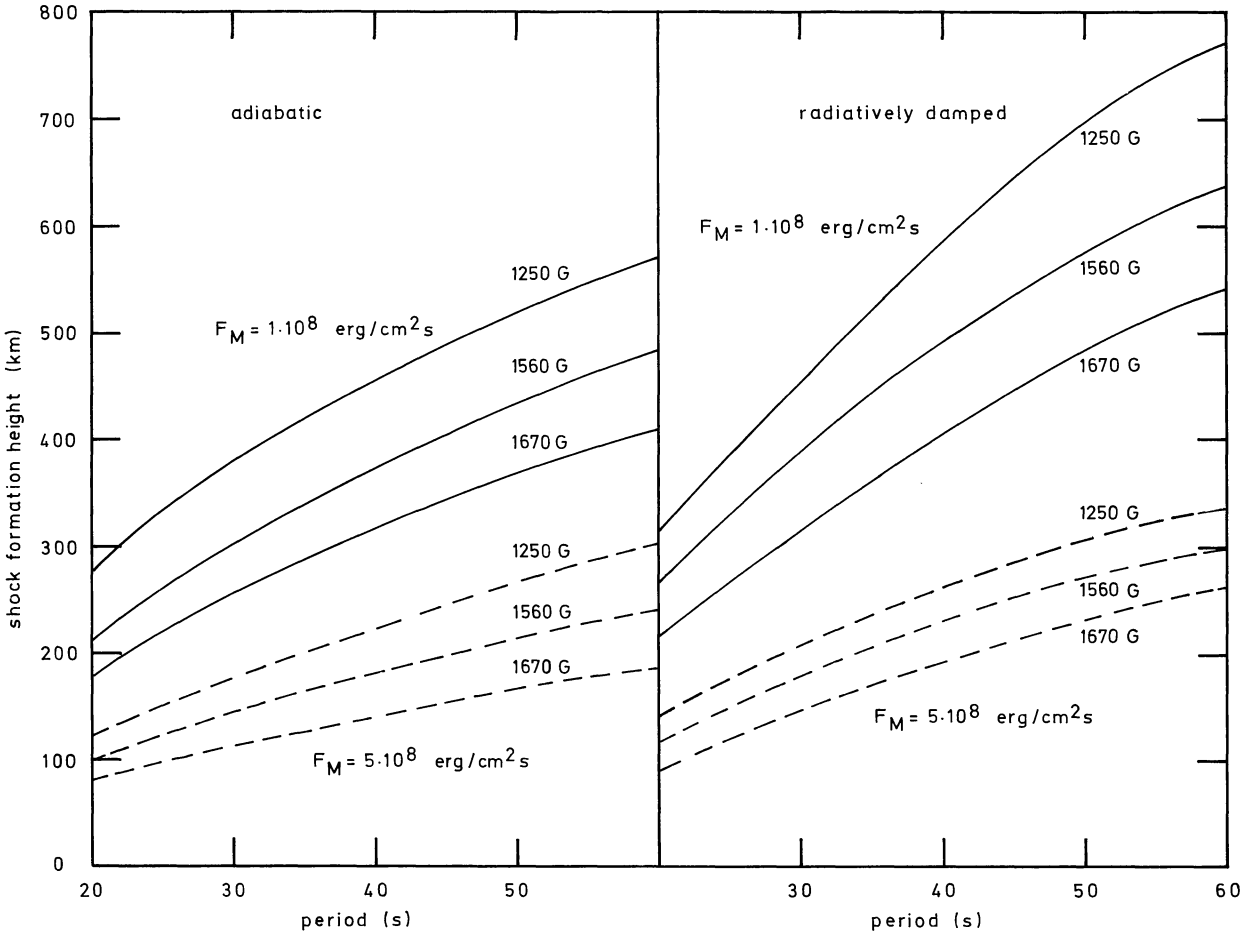

Fig. 9. Shock formation heights as function of wave period P and initial flux F_M far longitudinal tube waves in different flux tubes of indicated field strength B_{00} at the bottom of the tube. Left panel: adiabatic waves, right panel: radiatively damped waves

much smaller than the height z_0 where models A and B differ mainly the chromospheric behavior is affected by the different rates of spreading. Increased spreading distributes the mechanical energy over a greater cross-sectional area and thus decreases the relative wave amplitude as can be seen from a comparison of the velocities in Fig. 8. Decreased shock strength in turn leads to smaller dissipation and thus to lower mean temperatures $\bar{T}$ and pressures $\bar{p}$. Once shocks are formed spreading thus critically influences the chromospheric temperature rise and the pressure balance. In addition it is clear from our discussion of shock formation (Sect. 5.3, above) that for z_0 much smaller than 500 km shock formation itself could be accelerated (retarded) by a slower (faster) rate of spreading.

So far we have only discussed flux tubes with a fixed magnetic field strength $B_{00} = 1560$ G at the base. To show how a change in the magnetic field strength affects the non-linear behaviour of longitudinal tube waves we have constructed two other tube models. In model C, the field strength $B_{00} = 1250$ G has been chosen such that we have $c_A = c_S$ at the bottom of the tube, that is

$$p_{00} = \frac{2}{\gamma+2} p_{e0}, \tag{65}$$

while in model D the field strength is increased to $B_{00} = 1670$ G. From Eqs. (3) and (50) it is clear that the shape and the spreading of the flux tube in models C and D is the same as in model B. Together with B_{00}, the values p_{00} and ϱ_{00} are modified. Figure 9 shows the effect on the shock formation heights caused by the variation of field strength B_{00} in the tube for two different wave energies.

In model C and cases of small B_{00}, the density ϱ_{00} increases in the tube; thus, from Eq. (62), the velocity amplitude u_0 and the tube speed c_T decreases. This leads to shock formation at greater heights.

For model D and cases of high field strength B_{00}, we have $c_A \to \infty$, so that the tube becomes more and more rigid; the longitudinal waves thus go over the acoustic tube waves. With increasing B_{00} and thus decreasing density ϱ_{00} in the tube, the velocity amplitude u_0 of the wave [from Eq. (62)] increases, leading to shock formation at lower height (cf. Fig. 9). On the other hand, decreasing B_{00} leads to greater shock formation heights, less rigidity and thus greater disparity between longitudinal and acoustic tube waves.

6. Conclusions

We have compared longitudinal magneto-hydrodynamic flux tube waves with acoustic tube waves (which propagate in rigid tubes defined by the magnetic field boundary) and with ordinary acoustic waves in plane geometry. For the case of isothermal gravitationally-stratified atmospheres, phase relations are derived for the linear theory (Appendix A). Longitudinal tube waves

become acoustic tube waves when the distensibility, that is, the time dependent breathing of the flux tube is neglected. Acoustic tube waves in turn reduce to ordinary acoustic waves when the tube geometry, i.e. the spreading of the tube is neglected.

The time-dependent non-linear longitudinal tube wave equations were solved with the effect of radiation damping taken into account. We have derived Hugoniot relations valid for shock wave propagation in magnetic flux tubes which in the limit of vanishing distensibility go over to the ordinary Hugoniot relations.

The linear and non-linear computations both show that in the chromosphere longitudinal tube waves relative to ordinary acoustic waves have much reduced wave amplitudes (Figs. 3–6 and 8). This is due to the fact that the wave energy is spread over a with height increasing cross-sectional area. Decreasing shock amplitudes lead to smaller mechanical dissipation, but also to diminished radiation loss. Thus the time averaged chromospheric temperatures and pressures in the flux tube are reduced relative to the ordinary acoustic case of the same input flux. For longitudinal tube waves we find in addition that chromospheric heating expands the flux tube relative to its initial radiative equilibrium configuration (Fig. 2).

Due to the spreading of the tubes both longitudinal and acoustic tube waves form shocks at greater height than ordinary acoustic waves do (Fig. 7). This is caused by the small non-linear wave distortion resulting from the slow growth of the wave amplitude. The disparity in shock formation height is greatest for long period waves where the amount of spreading per wavelength is largest. The delayed shock formation and dissipation in longitudinal waves allows more wave energy to reach great heights where the density and consequently the emission is small. Thus the chromospheric temperature gradient steepens much more with increasing wave period than is the case for ordinary acoustic waves (Figs. 3–6).

Our grey LTE optically-thin method of treatment of radiation damping is more general than methods which use Newtons law of cooling and adopt constant values of the radiative relaxation time (see Appendix B). Yet even this improved radiation treatment is highly simplistic in chromospheric situations. Test calculations (Schmitz et al., 1985) have shown that the low density in flux tubes leads to strong non-LTE effects in the dominant H^- emitter. Similarly effects of resonance scattering and strong non-LTE effects are expected for the dominant Mg II and Ca II line emission of the middle chromosphere.

Thus a quantitative discussion of the chromospheric temperature and density stratification, as well as heating and cooling rates must await future investigations. Nevertheless the qualitative computations of our present work show that longitudinal tube waves readily transport mechanical energy to chromospheric heights and can dissipate it there through shocks. As the wave energy generation in flux tubes is much more efficient (Ulmschneider and Stein, 1982) and as the tube spreading allows the energy to be transported to great heights there seems to be a good case for longitudinal tube waves as a chromospheric heating mechanism.

Finally for solar type flux tubes it was found that longitudinal and acoustic tube waves are very similar (Fig. 7). The effect of the distensibility thus appears much less important than the effect of the tube spreading. If the magnetic field strength in the tube is increased longitudinal waves become identical to acoustic tube waves. Decreasing the field strength in the tube leads to increasing influence of the distensibility and acts to magnify the disparity between longitudinal and acoustic tube waves (Fig. 9).

Acknowledgement. This work was generously supported by the Deutsche Forschungsgemeinschaft (SFB 132). RR is partially supported by the NASA Solar-Terrestrial Theory Program (NAGW-79).

Appendix

A. Polarization factors in the linear theory

The solution of the longitudinal tube wave Eqs. (1) to (4) for linearized cases assuming adiabatic wave propagation in an isothermal atmosphere with temperature T_0 were first given by Defouw (1976) and subsequently generalized by Roberts and Webb (1978). For the density-, pressure-, velocity-, magnetic field-, and cross sectional perturbations the solutions are written, ψ being an arbitrary amplitude

$$\varrho' = \varrho_{00}\psi\tilde{\varrho}e^{-\frac{3z}{4H}}e^{i(\omega t - kz)}, \tag{A.1}$$

$$p' = p_{00}\psi\tilde{p}e^{-\frac{3z}{4H}}e^{i(\omega t - kz)}, \tag{A.2}$$

$$T' = T_0\psi\tilde{T}e^{\frac{z}{4H}}e^{i(\omega t - kz)}, \tag{A.3}$$

$$u = \psi\tilde{u}e^{\frac{z}{4H}}e^{i(\omega t - kz)}, \tag{A.4}$$

$$B' = B_{00}\psi\tilde{B}e^{-\frac{z}{4H}}e^{i(\omega t - kz)}, \tag{A.5}$$

$$A' = A_{00}\psi\tilde{A}e^{\frac{3z}{4H}}e^{i(\omega t - kz)}, \tag{A.6}$$

where H is the scale height and ϱ_{00}, p_{00}, B_{00}, A_{00} are values of the undisturbed atmosphere at the bottom of the flux tube. The values $\tilde{\varrho}$, $\tilde{p}$, $\tilde{T}$, $\tilde{u}$, $\tilde{B}$, and $\tilde{A}$ are polarization factors which following Hines (1960) can be written as non-trivial solutions of the characteristic equation

$$\tilde{\varrho} = -i\left(\frac{\gamma-1}{\gamma H}\frac{c_S^2}{c_A^2} + \frac{1}{4H}\right) + k, \tag{A.7}$$

$$\tilde{p} = i\frac{3\gamma-4}{4H} + \gamma k, \tag{A.8}$$

$$\tilde{T} = \tilde{p} - \tilde{\varrho} = i\frac{\gamma-1}{H}\left(\frac{3}{4} + \frac{c_S^2}{\gamma c_A^2}\right) + (\gamma-1)k, \tag{A.9}$$

$$\tilde{u} = \omega\left(1 + \frac{c_S^2}{c_A^2}\right) \tag{A.10}$$

$$\tilde{B} = -\tilde{A} = -\frac{c_S^2}{\gamma c_A^2}\tilde{p}, \tag{A.11}$$

where γ is the ratio of specific heats, c_S is the sound velocity and c_A the Alfvén velocity.

For the acoustic tube waves the solutions and polarization factors may be obtained from the limit $c_A \to \infty$. For cases with no gravity ($H \to \infty$), the polarization factors go over to those of Roberts and Webb [1978, Eq. (48), note the different sign of the propagation vector k]. For $\omega \to \infty$ one has $k \to \infty$ and the perturbations u, ϱ', p', A', T' are in phase, while B' is 180° out of phase. For $\omega \to \omega_c$, where ω_c is the cut-off frequency, one has $k \to 0$ and the perturbations T', p', A' lead u by 90° in phase, while u leads ϱ' and B' by 90° in phase. This situation is similar to that for the ordinary acoustic waves (Hines, 1960) except that for $\omega \to \omega_c$ the phase of p' is different by 180°. Phase and group velocities are similar to those of the ordinary acoustic wave case (Hines, 1960)

for purely vertical propagation. Like in the acoustic wave case the cut-off frequency ω_c is explained as the fundamental resonance of the entire tube, as is seen from the fact that

$v_{ph} \to \infty$ for $\omega \to \omega_c$.

B. Radiation treatments using Newton's law of cooling

The radiation treatments of Webb and Roberts (1980) and of Roberts (1983) use Newton's law of cooling

$$\left.\frac{dQ}{dt}\right|_{\text{Rad}} = -\frac{c_v}{\tau_R}(T_e - T) \tag{B.1}$$

and assume a constant radiative relaxation time τ_R. Here $\left.\frac{dQ}{dt}\right|_{\text{Rad}}$ is the net radiative cooling rate (erg g^{-1} s^{-1}) and c_v is the specific heat at constant volume.

Using Eqs. (5), (8), and (9) we have a more general law

$$\left.\frac{dQ}{dt}\right|_{\text{Rad}} = -T\left.\frac{dS}{dt}\right|_{\text{Rad}} = -4\kappa\sigma(T_e^4 - T^4) \tag{B.2}$$

The radiative relaxation time

$$\tau_R = \frac{c_v}{16\kappa\sigma T^3} \tag{B.3}$$

varies rapidly with height (cf. Ulmschneider 1971, Eq. (16) and Table 2). Assuming $T_e \approx T$ it is seen by expanding (B.2) that Newton's law of cooling is a special case of the more general formula (B.2).

References

Ayres, T.R.: 1981, *Astrophys. J.* **244**, 1064
Defouw, R.J.: 1976, *Astrophys. J.* **209**, 266
Edwin, P.M., Roberts, B.: 1983, *Solar Phys.* **88**, 179
Giovanelli, R.G., Livingston, W.C., Harvey, J.W.: 1978, *Solar Phys.* **59**, 49
Hammer, R., Ulmschneider, P.: 1978, *Astron. Astrophys.* **69**, 273
Hines, C.O.: 1960, *Canadian J. Phys.* **38**, 1441
Hollweg, J.V., Jackson, S., Galloway, D.: 1982, *Solar Phys.* **75**, 35
Kurucz, R.: 1979, *Astrophys. J. Suppl.* **40**, 1
Landau, L.D., Lifshitz, E.M.: 1959, Fluid Mechanics, Pergamon Press, London
Lighthill, J.: 1978, Waves in Fluids, Cambridge Univ. Press, Cambridge
Linsky, J.L.: 1980, *Ann. Rev. Astron. Astrophys.* **18**, 439
Parker, E.N.: 1979, Cosmical Magnetic Fields, Clarendon Press, Oxford, Chap. 8
Rae, I.C., Roberts, B.: 1982, *Astrophys. J.* **256**, 761
Roberts, B.: 1981, Physics of Sunspots, Sacramento Peak Obs. workshop, eds. L.E. Cram, J.H. Thomas
Roberts, B.: 1983, *Solar Phys.* **87**, 77
Roberts, B., Webb, A.R.: 1978, *Solar Phys.* **56**, 5
Roberts, B., Webb, A.R.: 1979, *Solar Phys.* **64**, 77
Rudinger, G.: 1969, Nonsteady Duct Flow, Dover, New York
Schmitz, F., Ulmschneider, P., Kalkofen, W.: 1985, *Astron. Astrophys.* (in press)
Spruit, H.C.: 1981a, The Sun as a Star, ed., S. Jordan, NASA SP-450, p. 385
Spruit, H.C.: 1981b, *Astron. Astrophys.* **98**, 155
Spruit, H.C.: 1982, *Solar Phys.* **75**, 3
Spruit, H.C., Zweibel, E.G.: 1979, *Solar Phys.* **62**, 15
Stenflo, J.O.: 1978, *Rep. Progr. Phys.* **41**, 865
Ulmschneider, P.: 1971, *Astron. Astrophys.* **14**, 275
Ulmschneider, P., Kalkofen, W., Nowak, T., Bohn, U.: 1977, *Astron. Astrophys.* **54**, 61
Ulmschneider, P., Schmitz, F., Kalkofen, W., Bohn, H.U.: 1978, *Astron. Astrophys.* **70**, 487 (=USKB 78)
Ulmschneider, P., Stein, R.F.: 1982, *Astron. Astrophys.* **106**, 9
Vaiana, G.S. et al.: 1981, *Astrophys. J.* **245**, 163
Webb, A.R., Roberts, B.: 1980, *Solar Phys.* **68**, 87
Wentzel, D.G.: 1979, *Astron. Astrophys.* **76**, 20
Wilson, P.: 1979, *Astron. Astrophys.* **71**, 9
Wilson, P.: 1980, *Astrophys. J.* **237**, 1008
Wilson, P.: 1981, *Astrophys. J.* **251**, 756
Zwaan, C.: 1978, *Solar Phys.* **60**, 213